Formation of nanostructured copper filaments in electrochemical deposition

Sheng Zhong,[1] Yuan Wang,[1] Mu Wang,[1,2,*] Min-Zhe Zhang,[1] Xiao-Bo Yin,[1] Ru-Wen Peng,[1] and Nai-Ben Ming[1]
[1]*National Laboratory of Solid State Microstructures and Department of Physics, Nanjing University, Nanjing 210093, China*
[2]*International Center for Quantum Structures, Chinese Academy of Sciences, Beijing 100080, China*
(Received 12 June 2002; revised manuscript received 24 February 2003; published 16 June 2003)

In this paper, we report in detail the studies of a different self-organized copper electrodeposition carried out in an ultrathin layer of $CuSO_4$ electrolyte. On a macroscopic scale, the morphology of the electrodeposit is fingerlike. Microscopically, each fingering branch consists of long, straight copper filaments with periodic corrugated nanostructures. Branching rate of the electrodeposit is significantly decreased, compared with the patterns grown in conventional systems. Detailed information of the growth environment in the ultrathin electrodeposition system is provided, the formation mechanism of the periodic nanostructures on the deposit filaments is explored, and the origin of the significant descent of branching rate of the electrodeposit is discussed.

DOI: 10.1103/PhysRevE.67.061601 PACS number(s): 81.15.Pq, 45.70.Qj, 79.60.Jv, 82.80.Fk

I. INTRODUCTION

Pattern formation in electrochemical deposition has attracted much attention in physics community since 1984, when Matsushita *et al.* [1,2] observed that the patterns of electrodeposit look quite similar to those generated by a computer model known as diffusion-limited aggregation (DLA) [3]. Since then, much effort has been devoted to investigate the pattern formation of electrodeposits, especially how and why the ramified feature is generated [4–15]. The ramified feature of electrodeposit is often ascribed to diffusive noise in interfacial growth [16]. It is suggested that the noise originates from statistical fluctuation of concentration, which may introduce a random flux between two equal-potentialed points, varying from time to time in both sign and magnitude due to the random nature of ion diffusion. In addition to the random diffusive noise, convection (both natural convection and electroconvection) and electric migration may also affect the deposit morphology [17–20]. It has been demonstrated that when electroconvection becomes sufficiently strong, neighboring deposit branches approach each other, eventually form a network pattern [18,21]. To suppress convection, thin cells are normally used in experiments. Yet, even so, the effect of either natural convection or electroconvection remains [19,22]. We once carried out electrodeposition in agarose gel in order to suppress convection [23]. Indeed, more regular deposit morphology has been observed. However, by introducing polymers into the system, convection is diminished on one hand, on the other hand, interfacial energy of the deposit is modified since the chemical environment becomes different. Therefore, it is difficult to identify whether the variation of deposit morphology is associated with the suppression of convection or with the change of interfacial energy. It would be ideal to find an experimental system in which convective disturbance is suppressed, at the same time no additional uncontrollable factors are introduced.

Apart from the interest in pattern formation research, understanding and control of deposit morphology may also be important for the applications in microelectronics. Nowadays, the integrated circuit industry has begun to switch rapidly from aluminum-based wiring to multilevel metal interconnects based on copper. This transition is due to the fact that the chips wired with copper have significant advantages in performance and manufacturing cost over those made with aluminum [24,25]. In microelectronics industry, the metallic interconnection is achieved via the photolithography process. To find new ways to form electric contacts in three dimensions and to achieve enhanced data-processing density, people have been trying to establish conducting channels between electrodes with patterned and direction-controlled electrodeposition [26,27] and electropolymerization [28,29]. For example, Bradley *et al.* report that the electrodissolution and electrodeposition processes in an applied electric field can be exploited to create directional growth of copper deposits between copper particles [27]. Yet in these reports the metal deposit is usually ramified, which may increase the electric capacitance of the system and cause delay in switching time. An essential step towards the real application of the direct electrodeposition method is to suppress ramification of the deposit and to get efficient control over the deposit morphology.

Recently we find a unique method to generate an ultrathin electrolyte layer for electrochemical deposition, in which the morphology of the deposits can be changed tremendously [30]. In this paper, we report in detail the formation of these different copper electrodeposits that grow robustly on glass substrate and have considerably low branching rate. In particular, we provide detailed information of the electrodeposition environment in the ultrathin electrolyte layer, which is essential to understand the self-organized pattern formation process therein. The influence of defects on the substrate in the development of the straight filaments is presented. In addition to structural and chemical analysis of the deposit filaments, the relation of the periodicity of nanostructures on the filaments and experimental parameters, the mechanisms for the decreased branching rate, and the origin of the spatiotemporal oscillations observed in the system, etc. are also discussed.

*Electronic address: muwang@netra.nju.edu.cn

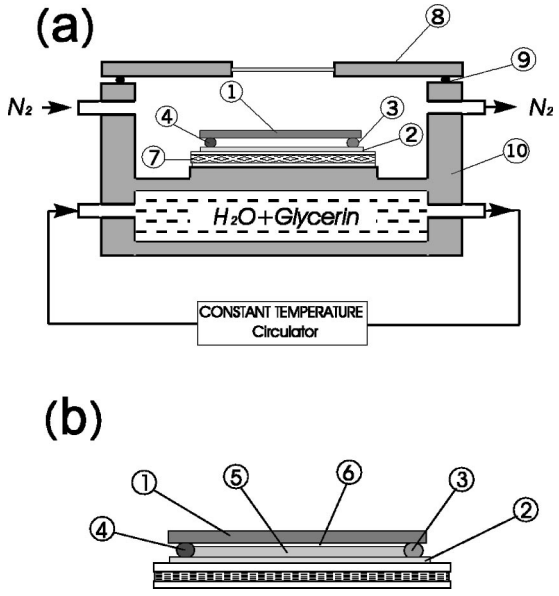

FIG. 1. (a) A schematic diagram of the experimental setup for the generation of the ultrathin electrolyte film and for the electrodeposition. The cell for electrodeposition shown here has two parallel electrodes. (b) The details of the electrodeposition cell with the parallel-electrode design. (1) Top glass plate; (2) bottom glass plate; (3) cathode; (4) anode; (5) ice of electrolyte; (6) ultrathin electrolyte layer trapped between the ice of electrolyte and the glass substrate; (7) Peltier element used for stimulating nucleation in solidifying the electrolyte; (8) top cover of the thermostated chamber with a glass window; (9) rubber O ring for sealing; (10) thermostated chamber to keep a constant temperature for electrodeposition.

II. EXPERIMENTAL SETUP AND METHODS

The electrodeposition was carried out in a cell made of two carefully cleaned glass plates. There were two types of geometrical arrangements for the electrodes. In one scenario, the anode was a circular ring and the cathode was a graphite needle, which was inserted through a small hole at the center of the upper glass plate, perpendicular to the plane of the anode, and touching the electrolyte layer beneath. Meanwhile, the electric field was centripetal. The ring anode was made of pure copper wire (99.9%, Goodfellow, UK) and the ring radius was 10 mm. The diameter of the cathode was 0.5 mm (the hole on the glass plate had the same size). For the other scenario, two parallel, straight electrodes were 8.0 mm apart and fixed on the bottom glass plate [31]. The electrode materials were the same as those for the circular cell. A schematic diagram of the experimental setup is shown in Fig. 1. The electrolyte of $CuSO_4$(0.05 M, pH$=4.5$) was confined in the space between the upper and the lower glass plates and the electrodes. The electrolyte solution was prepared by analytical reagent $CuSO_4$ and deionized, ultrapure water (electric resistivity 17.8 MΩ cm). No special treatments (such as coating with metal clusters [7,10]) were made on the glass surface except conventional cleaning. A Peltier element was placed beneath the electrodeposition cell to modify temperature. Both the deposition cell and the Peltier element were sealed in a thermostat chamber. Dry nitrogen flowed through the cell to prevent water condensation on the glass window, so *in situ* optical observation could be carried out. The temperature for electrodeposition was usually set to $-4\,^{\circ}$C for 0.05 M $CuSO_4$ solution, below the freezing point of the electrolyte.

To generate an ultrathin electrolyte layer for electrodeposition, we solidified the $CuSO_4$ solution by decreasing temperature. To achieve a large, flat electrolyte-solid interface, great care was taken in the beginning of solidification to keep only one or just a few ice nuclei in the system. Several melting-solidification cycles were repeated to fulfill this requirement. In our system, solidification started from the bottom glass plate. During solidification, $CuSO_4$ was partially expelled from the solid (this effect was known as partitioning effect [32–35] in crystallization). As a result, the concentration of $CuSO_4$ increased in front of the solid-electrolyte interface. Meanwhile, very low solidification rate had to be used in order to prevent the cellular interfacial morphology [36]. On the other hand, it is known that the temperature at which electrolyte solidifies (melting point/solidification point) depends on the concentration of electrolyte. For the electrolyte of $CuSO_4$, the solidification temperature decreases when the salt concentration is increased. Therefore, when the equilibrium was reached at a set temperature ($-4\,^{\circ}$C, for example), there existed an ultrathin layer of concentrated $CuSO_4$ electrolyte between the ice of electrolyte and the glass substrate. In our experiments, electrodeposition was carried out in this ultrathin layer, where the $CuSO_4$ concentration was expected not to exceed the saturated concentration of $-4\,^{\circ}$C (at $-4\,^{\circ}$C, the saturated concentration is about 0.7 M). The thickness of this ultrathin layer depended on the initial concentration of the electrolyte and the setting temperature. At $-4\,^{\circ}$C, this layer was around 200 nm in thickness (initial electrolyte concentration 0.05 M), which was based on the measurement of the thickness of copper electrodeposit with atomic force microscopy.

As indicated in Fig. 1(b), the electrodes were in contact with the concentrated ultrathin electrolyte layer trapped between the ice of electrolyte and the glass substrate. To verify the existence of this ultrathin layer and to test whether it was indeed in contact with the electrodes, we measured the electric resistance between the electrodes. In one case, we immersed two electrodes in a cup of electrolyte and solidified the electrolyte into ice. Whereas in the other case, the measurement was carried out in the setup shown in Fig. 1. The separation of the electrodes, the initial electrolyte concentration, and the temperature were the same for these two scenarios. It turned out that the resistance between the electrodes in the first case (bulk system) was several orders of magnitude higher than that in the second one. This suggests that for the electrodeposition setup shown in Fig. 1, there existed a layer of concentrated electrolyte connecting the two electrodes. Further evidence for the existence of such an ultrathin layer will be presented in Sec. IV.

In our experiments, both potentiostatic and galvanostatic designs generated similar deposit morphology. In the potentiostatic experiment, the constant voltage across the electrodes was selected between 1.0 V and 5.0 V. Meanwhile, the electric current in electrodeposition was recorded as a function of time. In galvanostatic experiments, the constant cur-

rent flowing through the deposition cell was in the range of 10 μA–100 μA and the voltage drop across the electrodes was recorded as a function of time.

The morphology of electrodeposit was observed with an optical microscope (Leitz Orthoplan-pol) and was further analyzed by an atomic force microscope (AFM) (Digital Instruments, Nanoscope IIIa) and a field-emission scanning electron microscope (LEO 1530). The structure and the chemical composition of the electrodeposit were analyzed with a transmission electron microscope (JEM-4000EX, JOEL).

III. EXPERIMENTAL RESULTS

Macroscopic morphology of the electrodeposit depends on the geometrical arrangement of the electrodes. For circular anode, fingering branches develop radially outwards, as shown in Fig. 2(a). Comparing to the previously reported dense-branching morphology [4–15], the most eye-catching feature of the electrodeposit shown here is that the branches become much more compact and have a fingerlike contour. The deposit has shiny metallic color and grows robustly on the glass substrate. For parallel electrodes, the fingering branches initiate from the cathode and develop towards the anode, as shown in Fig. 2(b). Comparing Figs. 2(a) and 2(b), no essential difference on the morphological details on this scale can be identified except the direction of branch development. Fingering in electrodeposition has been reported before [37], yet in our system the fingers distinguish themselves by their unique microstructures. Optical microscopy reveals that the fingering branches grown on the glass plate consist of long, narrow filaments, as shown in Fig. 2(c). The branching rate of the deposit has been significantly decreased comparing with previous ramified electrodeposits [4–15]. Isolated, straight filaments (more than 150 μm long) can be observed occasionally even though bifurcation does occur to most of the filaments. Screening effect, which is characterized by the termination of the deposit branch due to the competition for nutrient supply among the neighboring tips, can be observed in Fig. 2(c).

AFM reveals striking microscopic features of the copper filaments. As shown in Fig. 2(d), periodic corrugated structures exist on the filaments. The periodicity may vary from several tens of nanometers to a few microns depending on temperature, voltage or current applied across the electrodes, and pH of the electrolyte. The corrugated structures on the adjacent filaments are correlated in position, which can be easily identified in the region where the filament splits, as marked by the circles in Fig. 2(d). The corrugated structures mark the evolution of growth front in electrodeposition. AFM measurements show that the thickness of the electrodeposit is less than 200 nm, and the top surface of the deposit filaments is rounded [Fig. 2(d)], suggesting that the top surface is not confined by any rigid boundaries during the growth. This also implies that the thickness of the ultrathin electrolyte layer where the copper filaments develop should be of the order of 200 nm.

The periodic structures are generated simultaneously over all the deposit filaments and are associated with an oscillat-

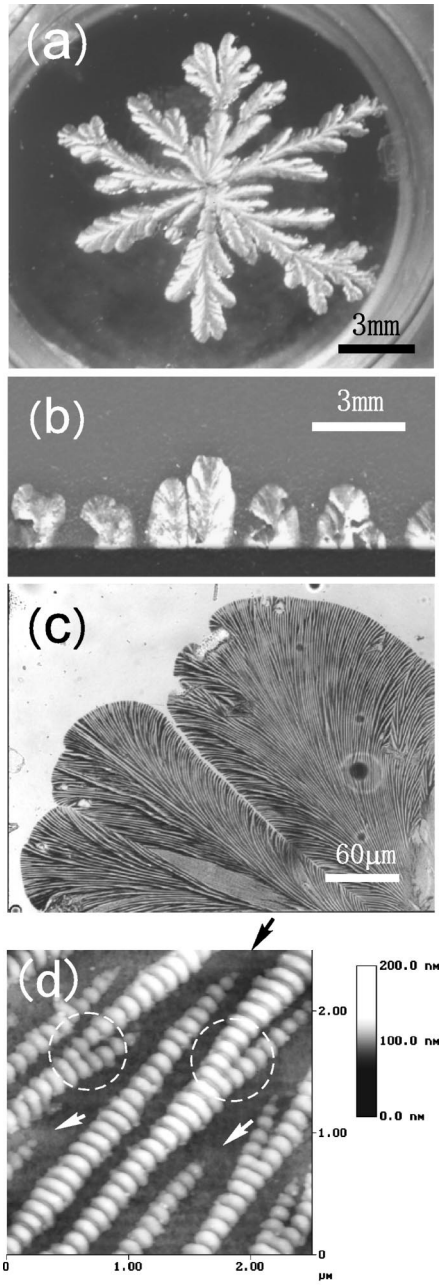

FIG. 2. (a) The macroscopic view of the electrodeposits of copper grown from a circular electrodeposition cell. The electrodeposit develops on the glass substrate with fingerlike branches. At the corners of the picture, the parts of the circular anode (pure copper wire) can be seen. The cathode is located in the center part of the deposit. (b) The electrodeposit generated in a cell with parallel electrodes. The black line at the bottom is the cathode. The fingerlike branches are similar to those formed in the circular cell. (c) Optical micrograph to show the detailed morphology of a fingerlike branch, in which long, narrow copper filaments can be identified. (d) The AFM view of the copper filaments. The periodic corrugated structures on the neighboring filaments are correlated in position, as indicated by the dashed circles in the regions where the splitting of the filaments takes place. One may find that no scratches exist in front of the filament tips, as indicated by the arrows. This fact suggests that the filaments were not following the scratches on the glass surface during the growth.

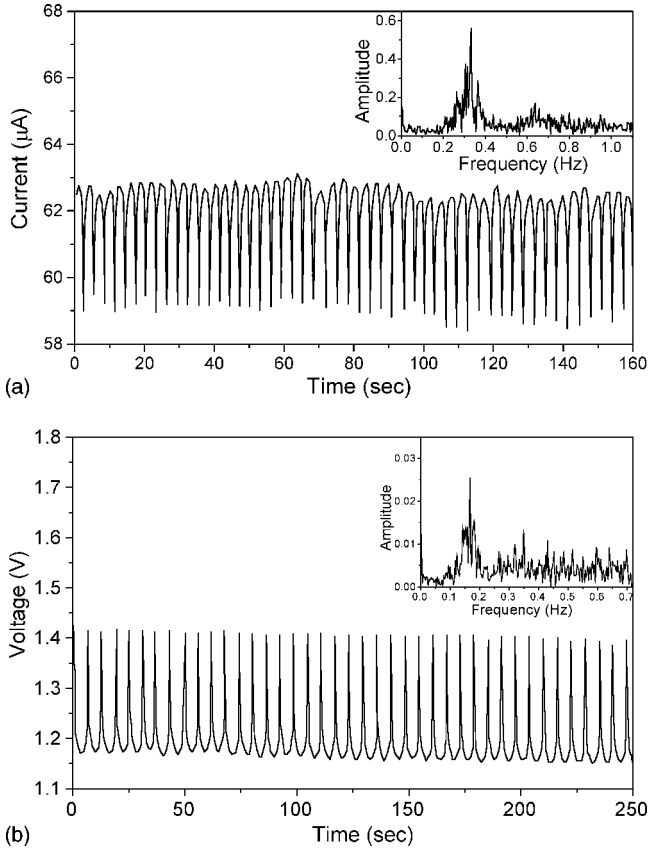

FIG. 3. (a) The oscillating electric current across the electrodeposition cell measured in a potentiostatic experiment. The inset is the Fourier transform of the oscillating current, which has a major peak at 0.33 Hz. (b) The oscillating voltage across the electrodes in a galvanostatic experiment. As indicated by the inserted Fourier transform of the oscillating voltage, a sharp peak exists at 0.17 Hz.

ing electric current or voltage. Figure 3(a) shows the oscillating electric current in a potentiostatic experiment. The insert of Fig. 3(a) is the Fourier spectrum of the oscillating current. It can be seen that the dispersion of the oscillation frequency is small and a distinct peak appears at 0.33 Hz. Figure 3(b) shows the oscillating voltage across the electrodes when the current during the electrodeposition was kept as a constant. The frequency of oscillation depends on the control parameters in experiments. Figure 4 shows a linear relation of the oscillation frequency and the current through the deposition cell (galvanostatic experiments). Figure 4 indicates that when the mass deposition rate becomes higher, the oscillation will be more intense. This implies that the oscillation should be transport dependent. Corresponding to the variation of temporal oscillation period, spatial period of the corrugated structures also changes. We investigated the dependence of the corrugated structure on the electric current in electrodeposition with galvanostatic mode. As illustrated in Figs. 5(a)–5(c), the spatial period of the corrugated structures decreases when the electric current is increased.

In our previous paper, we have shown that the corrugated structure on the filament is related to spontaneous alternating deposition of Cu_2O and copper [30]. The concentration of

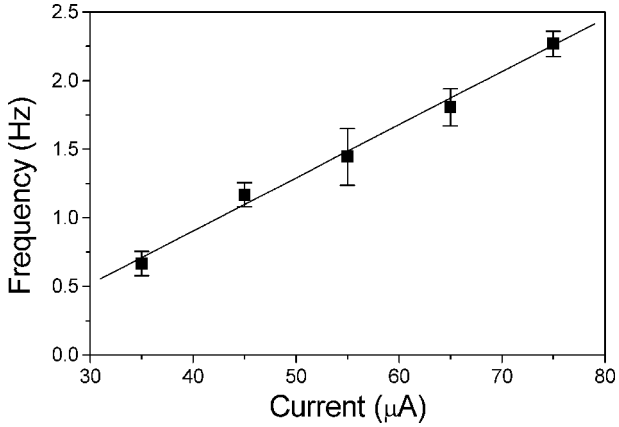

FIG. 4. Galvanostatic electrodepositions have been carried out at different electric currents. It has been observed that the oscillation frequency of the voltage across the electrodes increases linearly as the current is increased.

crystallite of Cu_2O is much higher in the ditch regions. This result has also been supported by the measurement of the conducting AFM with current mapping and current imaging tunneling spectroscopy. In current-sensing AFM measurements, we observed that the regions with stronger current and weaker current appear alternatingly, which correspond exactly to the periodic topographic variations. I-V curve in the regions with stronger current shows a nearly linear relation, whereas in the regions with weaker current a typical nonlinear I-V curve for semiconductor has been observed. Detailed analysis of the electric transport properties of the filaments will be reported separately [38].

IV. DISCUSSIONS

In order to understand the growth mechanism, it is essential to identify the growth environment where the unique electrodeposit presented above is generated. The electrodeposits develop on the surface of a flat glass substrate, which is one of the rigid boundaries of the electrolyte layer for electrodeposition. We emphasize that no prior modification has been made on the glass surface. The other rigid boundary in electrodeposition is the ice of $CuSO_4$ electrolyte. The shape of the ice-electrolyte interface may strongly affect the morphology of the electrodeposit. In solidifying the electrolyte, it is known that $CuSO_4$ is partially expelled from the solid due to the partitioning effect [32–35]. Meanwhile, a small amount of $CuSO_4$ is trapped in ice, whereas a large amount of $CuSO_4$ is accumulated in front of the ice, which forms a concentration gradient of $CuSO_4$. According to the solidification theory, this concentration gradient may lead to compositional supercooling [36]. Once this occurs, originally flat solid-liquid interface becomes unstable and a cellular pattern will be generated. Solidification theory shows that the formation of cellular pattern depends on the interfacial growth rate and the temperature gradient at the growing interface [36]. To avoid cellular interface, slow solidification rate and small temperature gradient are required [36]. When cellular pattern appears at the ice-liquid interface, the concentration of $CuSO_4$ within the ultrathin layer is no longer

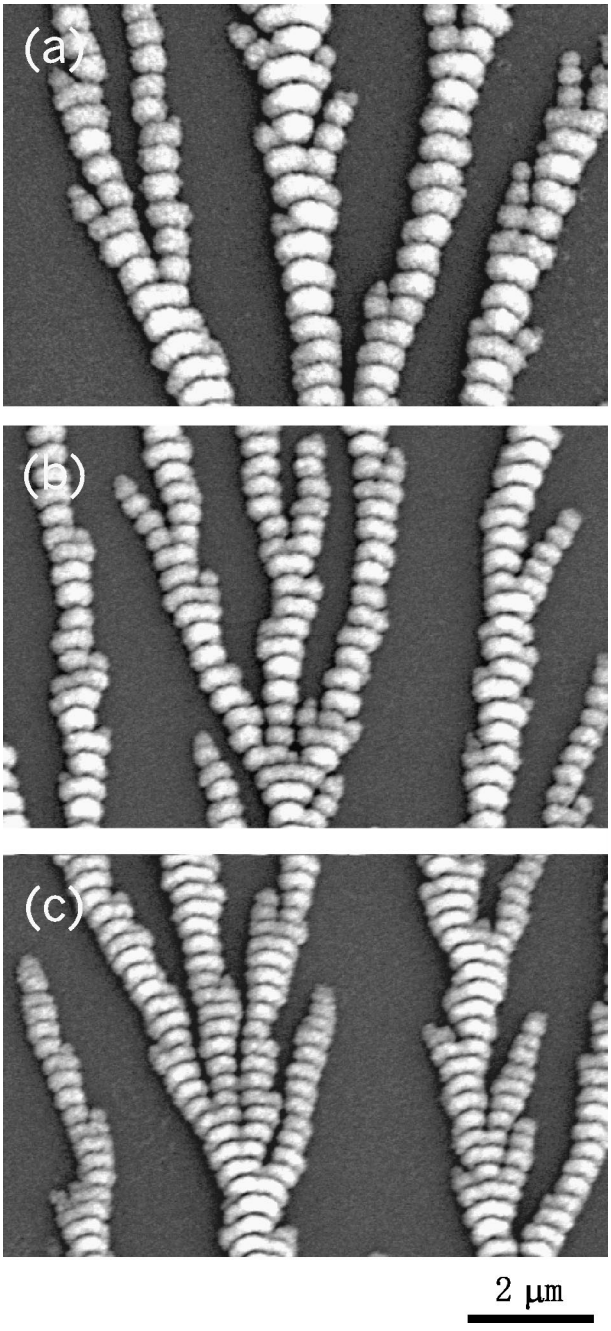

FIG. 5. SEM view of the filaments of the electrodeposit formed in different galvanostatic experiments. (a) 35 μA, (b) 47 μA, (c) 60 μA. One may find that when the current through the cell is increased, the spatial period of the corrugated structures decreases.

homogeneous horizontally. At the sites corresponding to the valley of the cellular pattern, $CuSO_4$ is richer than the other places. When electrodeposition is carried out in the valley region, the electrodeposit becomes thicker due to faster local deposition rate. At the sites corresponding to the bumps of the cellular pattern, the concentration of $CuSO_4$ is relatively lower and the electrolyte layer is thinner. Consequently, the electrodeposition process is slower and the deposit is thinner. To demonstrate this effect, we intentionally solidify the electrolyte with a high rate and hence introduce a cellular pattern

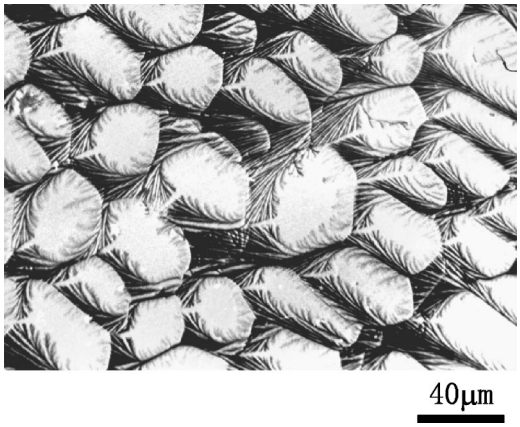

FIG. 6. When the solidification rate of the electrolyte is high, cellular structure can be formed on the ice-electrolyte interface. Meanwhile, in the valley region of the cellular structure, $CuSO_4$ concentration is higher and the electrolyte layer is thicker. Whereas in the region corresponding to the bump of the cellular pattern, the concentration of $CuSO_4$ is lower and the electrolyte layer is thinner. When electrodeposition is carried out in this inhomogeneous electrolyte layer, the deposit branches follow the track of the valleys and form a network pattern. The vacant regions in the above picture correspond to the bumps of the cellular ice-electrolyte interface, where the lower $CuSO_4$ concentration and much thinner space hinder the development of the deposit branches into these regions.

on the electrolyte-ice interface. When electrodeposition is carried out in this inhomogeneous electrolyte layer, electrodeposit branches follow the valleys, and eventually develop to a network, which outlines the distribution of the cellular on the electrolyte-ice interface, as shown in Fig. 6. This observation provides further evidence that the electrodeposition indeed takes place in the ultrathin electrolyte layer that is trapped between glass plate and ice of electrolyte.

It is interesting to know whether the defects on the glass surface itself, such as scratches, may affect the morphology of the electrodeposit. Generally the defects provide favorable sites for nucleation, so the deposit follows the shape of the defect. However, our observation indicates that our straight deposit filaments are not induced by the scratches on glass surface. Figure 7 illustrates the detailed morphology of deposit filaments observed by AFM. As indicated by the arrows, scratches can be identified on the substrate. Clearly, the filaments of the electrodeposit do not follow the scratches. Furthermore, one may find in both Figs. 7 and 2(d) that some branches would have grown forward if they were not screened by the neighboring filaments [for example, those illustrated by the arrows in Fig. 2(d)], yet no trace of scratches can be recognized on the substrate in front of the tips of the terminated filaments.

The most distinct difference of the electrodeposition shown here and those reported previously is that in our case, the branching rate of the electrodeposit has been decreased significantly. We previously suggested that strong electric migration versus slower diffusion was responsible for the formation of straight filaments [30]. To check the validity of this ''migration vs diffusion'' argument, we recently carried

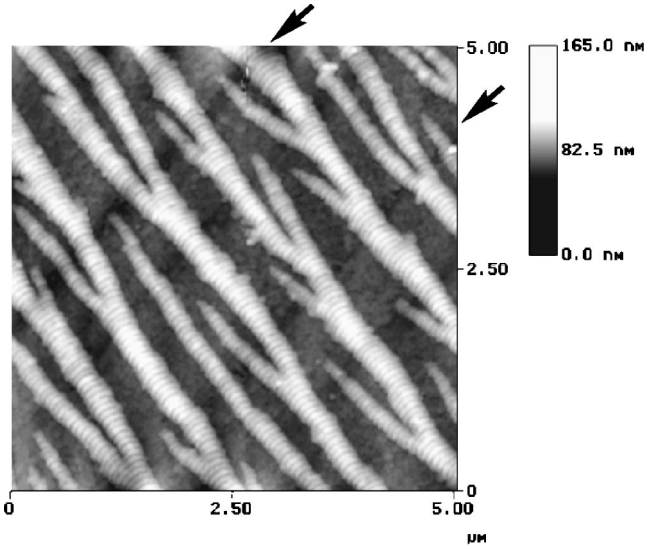

FIG. 7. AFM view of the morphology of the copper filaments grown on the glass surface with scratches (indicated by the arrows). One may find that the filaments of the electrodeposit do not necessarily follow the scratches.

out the replacement reaction in the ultrathin electrolyte layer of $CuSO_4$ with zinc wires. Thin wires of zinc are placed in the positions of previous copper and carbon electrodes. The solidification procedure of the electrolyte is the same as before. Meanwhile, the zinc wire contacts the electrolyte between the ice and the glass plate, and no external voltage or current is applied. So there should be no electric migration on macroscopic scale. To our surprise, the deposit generated in this replacement reaction is less random and ramified, as shown in Fig. 8(a). AFM reveals that the surface of the deposit branches is very smooth, as shown in Fig. 8(b). Whereas those generated in a much thicker electrolyte layer are very much random and ramified. These results strongly suggest that a strong electric migration may not be essential for the generation of straight, smooth filaments, and what we observed in the ultrathin layer electrodeposition is a noise-reduced effect. By reducing the layer thickness, convective noise in front of the growing interface (caused by both the natural convection and the electroconvection) is greatly suppressed, so the deposits become much more regular. It should be noted that in electrodeposition, the most front tips of electrodeposits are the ''hottest points'' for nucleation. According to the theory of Chazalviel [39], cation concentration behind the growing front virtually approaches zero. Once a nucleus appears and develops on the tip of the deposit filament, nucleation behind the tip becomes nearly impossible. All these factors ultimately lead to the electrodeposit filaments with a low branching rate.

It is true that at low temperature and high electrolyte concentration, viscosity of the electrolyte increases considerably, which may change the deposit morphology. Could a higher viscosity contribute to the smooth and straight deposit filaments? We checked this possibility by measuring the viscosity of $CuSO_4$ electrolyte as a function of temperature and the corresponding variation of deposit morphology. Our results indicated that by decreasing temperature from 30 °C to

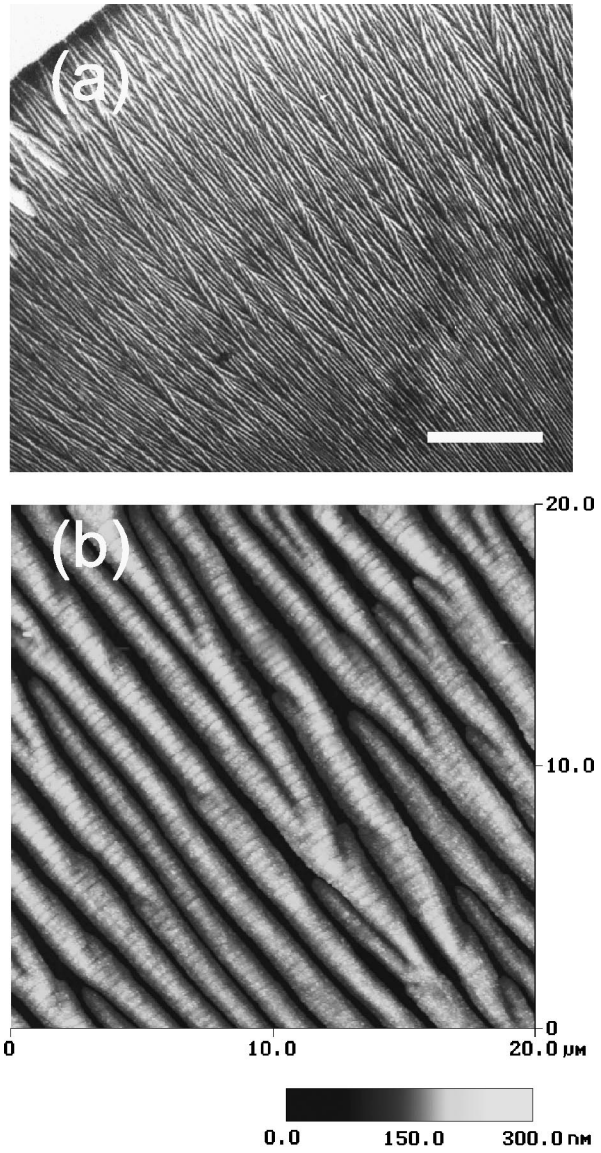

FIG. 8. The morphology of copper branches formed by replacement reaction from an ultrathin layer of $CuSO_4$ with a zinc wire. The branches grow on the glass plate and initiate from a zinc wire that is in contact with the ultrathin layer of electrolyte. (a) The copper branches observed with optical microscope. The bar represents 50 μm. (b) AFM micrograph of the copper branches shown in (a). One may find that no essential differences can be identified between those generated by replacement reaction and those formed by electrochemical deposition with an external electric power supply.

-5 °C, viscosity of the electrolyte changed from 0.855×10^{-3} Pa s to 2.135×10^{-3} Pa s. Corresponding to this nearly triple increase of viscosity, the deposit morphology also changed. Figure 9(a) illustrates the electrodeposits at 30 °C, and Fig. 9(b) shows the deposit grown at -5 °C in *supercooled* electrolyte solution. It should be emphasized that for both (a) and (b), the electrolyte remained in liquid state and the electrodeposition took place in the aqueous electrolyte layer sandwiched by glass plates, i.e., the electrodeposits floated in the electrolyte solution. The control

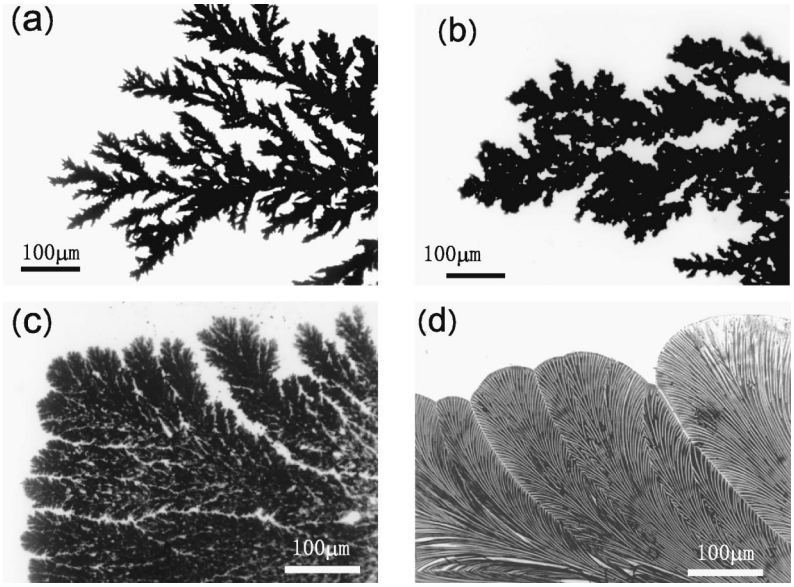

FIG. 9. The morphology of electrodeposits developed at different experimental conditions. (a) The copper electrodeposits grown at 30 °C in aqueous solution sandwiched by two glass plates; (b) the copper electrodeposits grown at −5 °C in supercooled aqueous solution sandwiched by two glass plates. The experimental conditions are the same for both (a) and (b) except for the temperature. (c) The copper electrodeposits grown on glass plate at −3 °C, just before the solidification of the electrolyte starts (i.e., in supercooled electrolyte solution). (d) The copper electrodeposits grown on glass plate at −3 °C when the electrolyte in the deposition cell has been solidified. The voltage across the electrodes is kept the same for both (c) and (d). We infer from (c) and (d) that the significant decrease of the thickness of the electrolyte layer plays a key role in decreasing the branching rate and the formation of much smoother electrodeposit filaments.

parameters for the formation of the deposits shown in Figs. 9(a) and 9(b), such as the electrolyte concentration, the electric current, and the geometric aspects of the electrodeposition cell, were kept the same except the temperature. It can be seen from Figs. 9(a) and 9(b) that with higher viscosity, the deposit branches were more condensed. The dendritic features became less evident at lower temperature. However, despite the difference on fine features, the patterns shown in both Figs. 9(a) and 9(b) were essentially dense-branching morphology.

Figure 9(c) shows the deposit grown on the surface of glass substrate at −3 °C in *supercooled* aqueous solution. Meanwhile, the thickness of the electrolyte was of the order of 300 μm. Figure 9(d) shows the deposit of copper grown on the surface of glass plate at −3 °C in the ultrathin electrolyte solution film when the solidification of electrolyte had taken place. The major differences of growth conditions for those shown in Figs. 9(c) and 9(d) were the layer thickness of the electrolyte and the electrolyte concentration. Indeed electrolyte concentration affected the deposit morphology [22], yet on a microscopic scale the deposits were always ramified and randomly branching. In our experimental system, the electrolyte concentration does not tremendously change the microscopic morphology of the deposit. The reason is that we carried out control experiments under a microscope by changing electrolyte concentration from 0.008 M to 0.8 M. Although macroscopic pattern of the deposits varied, under optical microscope the deposit branches were always dense branching. Whereas for the patterns shown in Figs. 9(c) and 9(d), the difference of the exact electrolyte concentration in front of the electrodeposit should be less than 20 times [40]. It is therefore unlikely that such a difference in concentration may be responsible for the completely different morphologies shown in Figs. 9(c) and 9(d). So we conclude that the significant decrease of the branching rate and the increase of regularity of the deposit shown in Fig. 9(d) are mainly due to the geometrical restriction of the ultrathin electrolyte layer, which efficiently suppresses the noise in electrodeposition.

The restriction of the thickness of electrolyte layer is also responsible for the periodic nanostructures on the filaments. The electrocrystallization of copper from the $CuSO_4$ solution can be understood as follows: First, Cu^{2+} ions are driven by electric field to the cathode. Then they are reduced and diffused on the deposit surface. Nucleation of the adsorbed copper atoms, followed by limited growth, gives rise to a crystallite agglomerate. According to the Nernst equation, equilibrium electrode potential of $Cu|Cu^{2+}$ increases when the concentration of Cu^{2+} ($[Cu^{2+}]$) builds up. Whereas, the deposition of copper takes place only when the cathode potential is lower than this equilibrium value. The equilibrium electrode potential for Cu_2O, however, is much higher than that for Cu. Therefore, for a wide range of the electrolyte concentration, Cu_2O is deposited with priority. Suppose that $[Cu^{2+}]$ is initially high at the growing interface. As a result, the equilibrium potential for copper deposition is also high. By applying a sufficiently low electrode potential to the cathode, both Cu and Cu_2O are deposited. It should be noted that the deposition rate of Cu_2O is proportional to the product of both $[Cu^{2+}]$ and $[OH^-]$ [41], whereas $[OH^-]$ is much lower than $[Cu^{2+}]$. Therefore, the deposition rate of the

semiconducting Cu_2O is very low compared to that of copper. The electrodeposition consumes Cu^{2+}, at the same time, the ion transport is confined by the geometrical restriction of the ultrathin electrodeposition system. Hence, $[Cu^{2+}]$ is lowered in front of the growing interface and it takes time for the Laplacian fields to compensate this descend. Meanwhile, the equilibrium electrode potential of Cu decreases and it may even become lower than the actual electrode potential. Once this occurs, the copper deposition stops, yet the deposition of Cu_2O remains. Note that Cu_2O deposits with a very low rate, which allows $[Cu^{2+}]$ in front of the growing interface being accumulated again. Consequently, the equilibrium electrode potential of Cu^{2+} resumes. When its value becomes higher than the actual electrode potential, copper deposition restarts. In this way copper filaments with periodically modulated concentration of Cu_2O, and hence periodic nanostructures are generated. It can be inferred that the periodicity of the compositional and topographic oscillations depends on the *p*H of the electrolyte, which has indeed been experimentally observed.

To summarize, we report in this paper the details of formation of nanostructured copper filaments in an ultrathin layer of $CuSO_4$ solution. The macroscopically fingering electrodeposit shown here differs from previous experimental observations in every microscopic detail. The most essential character of our electrodeposit is that the filaments become much smoother and more regular. The spatial period of the nanostructures on the filaments depends on the control parameters, such as the voltage or current in the electrodeposition. We suggest that the diffusive or convective noise at the growing interface is suppressed by strong confinement of the thickness of the electrolyte film, which eventually leads to the more regular filaments. In addition, a mechanism is proposed for the formation of periodic nanostructures on the deposit.

ACKNOWLEDGMENTS

This work was supported by projects from the the National Natural Science Foundation of China (Grant Nos. 19974014 and 10021001) and from the Ministry of Science and Technology of China (Grant No. G1998061410). The authors thank Q. Wu, V. Fleury, and L. Lam for helpful discussions.

[1] M. Matsushita, M. Sano, Y. Hayakawa, H. Honjo, and Y. Sawada, Phys. Rev. Lett. **53**, 286 (1984).
[2] M. Matsushita, Y. Hayakawa, and Y. Sawada, Phys. Rev. A **32**, 3814 (1985).
[3] T.A. Witten and L.M. Sander, Phys. Rev. Lett. **47**, 1400 (1981); Phys. Rev. B **27**, 5686 (1983).
[4] G. Gonzalez, G. Marshall, F.V. Molina, S. Dengra, and M. Rosso, J. Electrochem. Soc. **148**, C479 (2001).
[5] O. Younes, L. Zeiri, S. Efrima, and M. Deutsch, Langmuir **13**, 1767 (1997).
[6] M.Q. Lopez-Salvans, F. Sagues, J. Claret, and J. Bassas, Phys. Rev. E **56**, 6869 (1997).
[7] V. Fleury, and D. Barkey, Europhys. Lett. **36**, 253 (1996).
[8] S.N. Atchison, R.P. Burford, and D.B. Hibbert, J. Electroanal. Chem. **371**, 137 (1994).
[9] F. Texier, L. Servant, J.L. Bruneel and F. Argoul, J. Electroanal. Chem. **446**, 189 (1998).
[10] V. Fleury, Nature (London) **390**, 145 (1997).
[11] D.P. Barkey, D. Watt, Z. Liu, and S. Raber, J. Electrochem. Soc. **141**, 1206 (1994).
[12] J.R. Melrose, D.B. Hibbert, and R.C. Ball, Phys. Rev. Lett. **65**, 3009 (1990).
[13] M.Q. Lopez-Salvans, F. Sagues, J. Claret, and J. Bassas, J. Electroanal. Chem. **421**, 205 (1997).
[14] O. Zik and E. Moses, Phys. Rev. E **53**, 1760 (1996).
[15] S.N. Atchison, R.P. Burford, C.P. Whitby, and D.B. Hibbert, J. Electroanal. Chem. **399**, 71 (1995).
[16] T. Vicsek, *Fractal Growth Phenomena*, 2nd ed. (World Scientific, Singapore, 1992), and references therein.
[17] V. Fleury, J. Kaufman, and D.B. Hibbert, Nature (London) **367**, 435 (1994).
[18] M. Wang, W.J.P. van Enckevort, N.-B. Ming, and P. Bennema, Nature (London) **367**, 438 (1994).
[19] J.M. Huth *et al.*, Phys. Rev. E **51**, 3444 (1995).
[20] J.R. de Bruyn, Phys. Rev. Lett. **74**, 4843 (1995).
[21] K.-Q. Zhang *et al.*, Phys. Rev. E **61**, 5512 (2000).
[22] F. Sagues, M.Q. Lopez-Salvans, and J. Claret, Phys. Rep. **337**, 97 (2000).
[23] M. Wang, N.-B. Ming, and P. Bennema, Phys. Rev. E **48**, 3825 (1993).
[24] D. Edelstein *et al.*, Tech. Dig. - Int. Electron Devices Meet. **1997**, 773 (1997).
[25] S. Venkatesan *et al.*, Tech. Dig. - Int. Electron Devices Meet. **1997**, 769 (1997).
[26] C. Gurtner and M.J. Sailor, Adv. Mater. (Weinheim, Ger.) **8**, 897 (1996).
[27] J.-C. Bradley *et al.*, Nature (London) **389**, 268 (1997).
[28] C.L. Curtis, J.E. Ritchie, and M.J. Sailor, Science **262**, 2014 (1993).
[29] M.J. Sailor and C.L. Curtis, Adv. Mater. (Weinheim, Ger.) **6**, 688 (1994).
[30] M. Wang *et al.*, Phys. Rev. Lett. **86**, 3827 (2001).
[31] S. Zhong *et al.*, J. Phys. Soc. Jpn. **70**, 1452 (2001).
[32] A.A. Chernov, *Modern Crystallography III: Crystal Growth* (Springer-Verlag, Berlin, 1984).
[33] N.-B. Ming, *Fundamentals of Crystal Growth Physics* (Shanghai Science and Technology, Shanghai, 1982).
[34] W. Kurz and D.J. Fisher, *Fundamentals of Solidification*, 4th ed. (Enfield Publishing & Distribution Company, Enfield, NH, 2001).
[35] A. Pimpinelli and J. Villain, *Physics of Crystal Growth* (Cambridge University Press, Cambridge, 1998).
[36] Consider the solidification of electrolyte by cooling the bottom plate of the system. The ice nucleus appears on the bottom plate and develops upwards. According to the theory of solidification, a part of the salt is expelled from the ice and the salt

concentration inside the ice is $k_o C_o$, where k_o is the equilibrium partitioning coefficient. Due to the partitioning effect, salt concentration in front of the growing interface becomes high, which influences the local solidification temperature (melting point) by $T(C_L)=T_o+mC_L(z)$, where T_o is the solidification temperature without any salt (pure water), $C_L(z)$ is the salt concentration field, and m is a negative parameter for $CuSO_4/H_2O$ system. From the above equation and the concentration field $C_L(z)$, one may easily find that there exists a region of compositional supercooling in front of the growing interface, if $(G/v)<[mC_L(k_o-1)]/Dk_o$ is satisfied, where G is the temperature gradient in z direction, v is the interfacial growth rate, and D is the diffusuion coefficient. This criterion indicates that when the other control parameters are fixed, compositional supercooling and hence cellular pattern can be easily induced if solidification rate of ice is high. In other words, in order to keep a flat growing interface, a slow solidification rate is usually required. Details can be found in Refs. [34,35].

[37] M.Q. Lopez-Salvans *et al.*, Phys. Rev. Lett. **76**, 4062 (1996).

[38] Yuan Wang *et al.* (unpublished).

[39] J.-N. Chazalviel, Phys. Rev. A **42**, 7355 (1990).

[40] At $-4\,^{\circ}C$ the saturated concentration of $CuSO_4$ is about 0.7 M, higher than this concentration crystallites of $CuSO_4$ may nucleate. In our experiment, the initrial concentration of $CuSO_4$ is 0.05 M. Therefore, the concentration difference for that in Figs. 9(c) and 9(d) should be around 14 times.

[41] E.W. Bohannan *et al.*, Langmuir **15**, 813 (1999).